# An automated method for thermal-optical separation of aerosol organic/elemental carbon for $^{13}C$ analysis at the sub-μgC level

Yao, Peng; Ni, Haiyan; Paul, Dipayan; Masalaite, Agne; Huang, Ru Jin; Meijer, Harro A.J.; Dusek, Ulrike

*Published in:*
Science of the Total Environment

*DOI:*
10.1016/j.scitotenv.2021.150031



*Publication date:*
2022

Science of the Total Environment 804 (2022) 150031

Contents lists available at ScienceDirect

Science of the Total Environment

journal homepage: www.elsevier.com/locate/scitotenv

# An automated method for thermal-optical separation of aerosol organic/elemental carbon for $^{13}C$ analysis at the sub-μgC level: A comprehensive assessment

Peng Yao [a], Haiyan Ni [a,b], Dipayan Paul [a], Agne Masalaite [c], Ru-Jin Huang [b,*], Harro A.J. Meijer [a], Ulrike Dusek [a,*]

[a] Centre for Isotope Research (CIO), Energy and Sustainability Research Institute Groningen (ESRIG), University of Groningen, Groningen 9747AG, the Netherlands
[b] State Key Laboratory of Loess and Quaternary Geology, Center for Excellence in Quaternary Science and Global Change, Key Laboratory of Aerosol Chemistry & Physics, Institute of Earth Environment, Chinese Academy of Sciences, Xi'an 710061, China
[c] State Research Institute Center for Physical Sciences and Technology, Vilnius, Lithuania

## HIGHLIGHTS

- $^{13}C$ analysis of EC at the sub-μgC level is achieved by the TOA-IRMS system.
- OC/EC separation and possible effects on the isotopic composition were evaluated.
- EC can be well isolated for $^{13}C$ analysis using the thermal-optical split point.
- Incomplete isolation of EC can bias dual isotope source apportionment.

## GRAPHICAL ABSTRACT

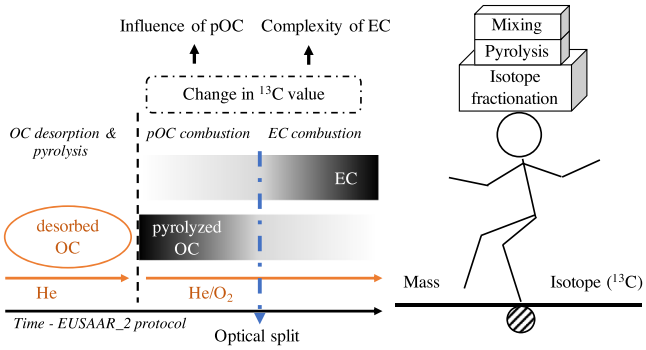


## ARTICLE INFO

*Article history:*
Received 8 July 2021
Received in revised form 17 August 2021
Accepted 26 August 2021
Available online 1 September 2021

Editor: Pingqing Fu

*Keywords:*
Elemental carbon
$^{13}C$ analysis
Automated method
Pyrolysis
Isotope fractionation

## ABSTRACT

We describe and thoroughly evaluate a method for $^{13}C$ analysis in different fractions of carbonaceous aerosols, especially elemental carbon (EC). This method combines a Sunset thermal-optical analyzer and an isotope ratio mass spectrometer (IRMS) via a custom-built automated separation, purification, and injection system. Organic carbon (OC), EC, and other specific fractions from aerosol filter samples can be separated and analyzed automatically for $^{13}C$ based on thermal-optical protocols (EUSAAR_2 in this study) at sub-μgC levels. The main challenges in isolating EC for $^{13}C$ analysis are the possible artifacts during OC/EC separation, including the premature loss of EC and the formation of pyrolyzed OC (pOC) that is difficult to separate from EC. Since those artifacts can be accompanied with isotope fractionation, their influence on the stable isotopic composition of EC was comprehensively investigated with various test compounds. The results show that the thermal-optical method is relatively successful in OC/EC separation for $^{13}C$ analysis. The method was further tested on real aerosols samples. For biomass-burning source samples, (partial) inclusion of pOC into EC has negligible influence on the $^{13}C$ signature of EC. However, for ambient samples, the influence of pOC on the $^{13}C$ signature of EC can be significant, if it is not well separated from EC, which is true for many current methods for measuring $^{13}C$ on EC. A case study in Xi'an, China, where pOC is enriched in $^{13}C$ compared to EC, shows that this can lead to an overestimate of coal and an underestimate of traffic emissions in isotope-based source apportionment.



* Corresponding authors.
*E-mail addresses:* rujin.huang@ieecas.cn (R.-J. Huang), u.dusek@rug.nl (U. Dusek).

https://doi.org/10.1016/j.scitotenv.2021.150031
0048-9697/

## 1. Introduction

Carbonaceous compounds are a major fraction of ambient aerosols in various environments (Huang et al., 2014; Fuzzi et al., 2015; Tao et al., 2017), and have been widely studied due to their climate and health effects. The total carbon (TC) content of carbonaceous aerosol can be sub-divided into organic carbon (OC) and elemental carbon (EC), where OC is carbon in organic compounds with various molecular sizes and EC is carbon in graphite or other carbon crystals (Petzold et al., 2013). OC can be emitted as primary particles from combustion sources (Chen et al., 2005; Habib et al., 2008) and be formed as secondary particles from oxidation of biogenic and anthropogenic volatile organic compounds (Kroll and Seinfeld, 2008; Hallquist et al., 2009). On the other hand, EC has only primary sources, produced in high-temperature combustion processes, mainly through solid fuel (coal or biomass) combustion and traffic emissions (Andreae and Gelencsér, 2006; Andersson et al., 2015).

The separation and quantification of OC and EC is inherently difficult, and various methods result in different separation. Currently, there are three main kinds of methods used: thermal methods combining inert and oxidizing conditions, thermal methods in an oxidizing atmosphere, and thermal-optical methods with inert and oxidizing conditions. Thermal methods combining inert and oxidizing conditions first desorb OC under inert conditions (He or $N_2$), and then combust the remaining carbon in oxygen and characterize it as EC. However, during desorption some parts of OC may form pyrolyzed OC (pOC), which later evolves during the EC step and thus is classified as EC. To solve this problem, thermal-optical protocols have been designed, such as EUSAAR_2 (Cavalli et al., 2010), IMPROVE (Chow et al., 2001), NIOSH 5040 (Birch and Cary, 1996), to correct for the contribution of light-absorbing pOC to EC. For example, in the EUSAAR_2 protocol, the pOC is determined based on the change of a laser signal transmitted through the filter. Specifically, the laser transmission signal first decreases due to OC pyrolysis under inert conditions and then increases as pOC and then EC are combusted in the oxidizing atmosphere. The OC/EC split is set at the time, when the laser transmission signal again reaches the initial value. Finally, the thermal methods in oxidizing atmosphere are designed to minimize pOC formation and combust OC directly in oxygen at relatively low temperature, e.g., 375 °C in the CTO-375 protocol (Zencak et al., 2007), and then combust EC in oxygen at higher temperature. These are mainly used for isolation of EC for radiocarbon ($^{14}C$) analysis.

Stable carbon isotope ($^{13}C$) analysis has long been used for aerosol source apportionment (Cachier et al., 1985; Norman et al., 1999), taking advantage of different $^{13}C$ signatures for main aerosol sources (Smith and Epstein, 1971; Widory, 2006). More recently, studies have focused on $^{13}C$ signatures of different carbon fractions, such as TC, OC, EC, water-soluble OC (WSOC), and other specific carbonaceous compounds (Fu et al., 2012; Andersson et al., 2015; Masalaite et al., 2018; Han et al., 2020). OC has many potential sources, and the $^{13}C$ signature of OC can be changed by atmospheric processes (Pavuluri and Kawamura, 2012; Kirillova et al., 2013). Therefore, chemical tracers or factor analysis of organic mass spectra are more commonly used for OC source apportionment (Zhang et al., 2017). Different from OC, EC only forms in combustion processes and the EC sources are therefore limited to coal burning, biomass burning (C3 and C4 plants), and traffic emissions. In addition, EC is chemically inert in the atmosphere (Schauer et al., 2003), making EC a good tracer of primary emissions. However, $^{13}C$ analysis of EC alone can give only a qualitative indication of sources rather than a quantitative source apportionment (Martinsson et al., 2017). Radiocarbon ($^{14}C$) analysis enables a clear distinction between contemporary and fossil carbon (Szidat et al., 2004; Gustafsson et al., 2009). Applying $^{14}C$ and $^{13}C$ analysis allows to separate the EC sources quantitatively (Chen et al., 2013; Andersson et al., 2015; Ni et al., 2018).

$^{13}C$ analysis with reliable OC/EC separation has therefore become increasingly important. Different methods have been applied to carbon isotope analysis, including thermal methods combining inert and oxidizing steps (Cao et al., 2011; Kawashima and Haneishi, 2012; Guo et al., 2016), thermal methods in oxidizing atmosphere (Zhang et al., 2012; Dusek et al., 2014), thermal-optical methods (Huang et al., 2006; Gustafsson et al., 2009; Chen et al., 2013; Andersson et al., 2015), sometimes after water extraction (Fisseha et al., 2009). However, the effects of these different methods on the carbon isotope composition of EC have not been fully characterized, including the thermal-optical methods. For these, the optical OC/EC split was originally introduced as a way to compensate for pOC formation, but not as a physical separation of OC and EC and it is not completely clear to which extent EC is separated from pOC at the split point. Apart from pOC formation, isotope fractionation can also happen in chemical and physical processes involved in OC/EC separation, which may lead to different $^{13}C$ values depending on the separation protocol. The challenges of thermal-optical OC/EC separation for $^{13}C$ analysis can be classified into the following categories. First, if all or part of pOC is classified as EC (by using no split point, or if the split time is too early), EC will have an altered $^{13}C$ signature due to mixing. On the other hand, if a part of EC is lost (too late split time), EC might have altered $^{13}C$ signature due to the kinetic isotope effect. Second, thermal desorption and pyrolysis may cause isotopic fractionation, which means different $^{13}C$ values in desorbed OC and pOC. Third, for methods minimizing the formation of pOC by combustion in pure $O_2$ at relatively low temperatures, a small but consistent loss of EC in pure $O_2$ changes the $^{13}C$ value of the remaining EC through isotope fractionation (Zhang et al., 2012; Dusek et al., 2014). A certain degree of mixing of pOC into EC or EC being combusted before the split point may be acceptable (and unavoidable), but it is important to better understand the related processes and the effects on isotopic composition of EC.

In our laboratory, an automated system is in use to analyze $^{13}C$ of OC by desorption in an inert atmosphere (Dusek et al., 2013; Zenker et al., 2020). In this work, this automated system is modified to enable the thermal-optical analysis of $^{13}C$ in EC. Most methods for $^{13}C$ analysis in EC described in the literature are offline (Huang et al., 2006; Gustafsson et al., 2009; Fisseha et al., 2009; Cao et al., 2011; Chen et al., 2013), where glass containers or flame-sealed tubes are needed to store $CO_2$ for independent $^{13}C$ analysis. In this method, the carbonaceous fractions are sequentially separated, combusted, purified, and immediately analyzed for $^{13}C$, avoiding any manual transfer of $CO_2$. Since the problems of online combustion and purification have been solved, the transfer interface should be applicable to online measurements and possible field instruments. In the first part of this work, the OC/EC separation, including pyrolysis and isotopic fractionation, is evaluated using different organic materials and their mixtures with carbon black (a surrogate of EC). The method is then applied to biomass-burning source samples and ambient aerosol samples, and finally in a $^{13}C$-$^{14}C$ source apportionment sensitivity study.

## 2. Materials and methods

### 2.1. System and method description

Our system consists of a Sunset thermal-optical analyzer (TOA, Sunset Laboratory Inc.) coupled to a continuous flow IRMS (652 Optima, VG, Isoprime) via a custom-built interface for sample separation, combustion, $CO_2$ collection, and purification. Specific fractions of carbonaceous aerosols are converted to $CO_2$ in the TOA (Fig. S1).

The interface schematic of the TOA-IRMS automated system is shown in Fig. 1a. In Mode 1, $CO_2$ produced from OC and EC is first flushed through a drier (SICAPENT, Merck), and then captured in a liquid nitrogen trap. After that, the 6-port valve is switched, and the system is changed into Mode 2. The $CO_2$ is transferred from the first liquid nitrogen trap to the concentrating trap (also liquid nitrogen, silicon capillary with small diameter). Finally, the $CO_2$ sample is transferred from the concentrating trap through a reduction oven

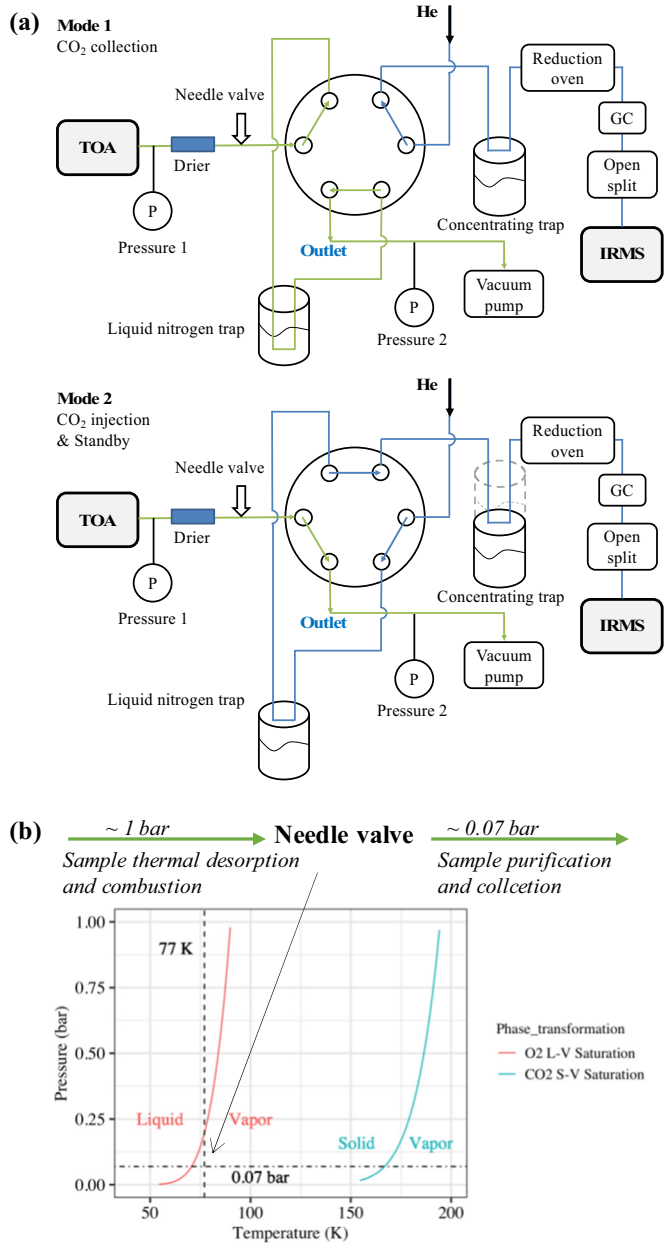


**Fig. 1.** (a) Schematic of the Sunset thermal-optical analyzer (TOA) - IRMS system (transfer interface) and operation modes. The green lines refer to the sample gas flow from the TOA. The blue lines refer to the He carrier gas flow which transports the purified sample into the IRMS. Mode 1 is the capturing of $CO_2$, and Mode 2 is the transfer of $CO_2$ and $^{13}C$ measurement. (b) Pressure control for online combustion and purification based on $O_2$ Liquid-Vapor (L-V) saturation and $CO_2$ Solid-Vapor (S-V) saturation.

(filled with copper and silver) and a gas chromatography column (GC, Agilent Technologies Inc.) into the IRMS via a custom-made open-split interface. The reduction oven and the GC column are used to eliminate the influence of interfering gases (e.g., $N_2O$ and $NO_2$).

The thermal-optical protocols use an oxidizing atmosphere (10% $O_2$ in He) to combust EC. Oxygen is necessary for the combustion of EC, but substantial quantities of oxygen can co-freeze in the liquid nitrogen trap at ambient pressures, causing a pressure shock to the system upon warming of the trap. In addition, the presence of oxygen in the carrier gas was found to shift the measured $\delta^{13}C$ values (the exact reason is not entirely clear, and it may be related to the ionization zone of the IRMS). To prevent the collection of oxygen, a needle valve is installed after the drier, and a vacuum pump is installed after the first liquid nitrogen trap. This allows the sample desorption and combustion at a pressure slightly above atmospheric (before the needle valve), while the $CO_2$ collection and purification in the liquid nitrogen trap is achieved at a much lower pressure (0.02–0.07 bar, after the needle value), as is shown in Fig. 1b. The vapor pressure of $O_2$ is around 0.2 bar at 77 K, so $O_2$ will not freeze in the liquid nitrogen trap below 0.07 bar, whereas $CO_2$ can be well captured. More details about the operating process can be found in Supporting Information Section S1.

### 2.2. Thermal desorption protocol

As the transition from OC to EC is gradual, it is not possible to isolate EC unambiguously for isotopic analysis, and several approaches are used in the literature. In this work, the EUSAAR_2 protocol (Cavalli et al., 2010) is used to isolate EC (Table S1). The aerosol sample is heated first in several temperature steps in an inert He atmosphere to volatilize OC, and later in several temperature steps in an oxygen-rich atmosphere ($He/O_2$) for combustion of pOC and EC. The laser transmittance (Diode laser, 658 nm) through the filter is used to quantify pOC formation (Fig. S1). The laser transmittance first decreases due to pOC formation in He and then increases as pOC (potentially along with some native EC) is combusted in $He/O_2$. The moment that the laser transmittance signal arrives back at the original value is defined as OC/EC split point. Filters were analyzed in two steps: the first OC/EC analysis is used to determine the split time, and at the same time all evolved $CO_2$ is captured for $^{13}C$ analysis of TC. The second run only captures our best estimate of EC, namely the carbon fraction evolved after the recorded split time. While this does not guarantee 100% physical separation of pyrolyzed carbon from native EC, pOC is likely combusted at lower temperatures than the majority of EC, because of its formation by pyrolysis at low temperatures. To avoid ambiguity, pOC in this study specifically refers to the carbon fraction evolved between the start of the $He/O_2$ phase and the split time in EUSAAR_2 protocol, and EC refers to the fraction captured after the split time. To avoid traces of oxygen in the trap, the EUSAAR_2 protocol is modified with an extra He flushing step (Table S1). A thermogram of an ambient aerosol sample can be found in Fig. S2 as an example.

### 2.3. $^{13}C$ measurement and correction

$^{13}C/^{12}C$ ratios are reported in the so-called delta notation ($\delta^{13}C$). The $\delta^{13}C$ values are calculated as the relative difference between the $^{13}C/^{12}C$ ratio ($R^{13}$) of the sample and that ratio of the international primary standard Vienna Pee Dee Belemnite (VPDB):

$$\delta^{13}C = \frac{R^{13}_{Sample}}{R^{13}_{VPDB}} - 1 \quad (1)$$

In our laboratory, the $\delta^{13}C$ values of samples are calibrated by a three-point linear fit based on two local reference materials CAN (isotopically enriched caffeine, $\delta^{13}C = 0.61‰ \pm 0.10‰$) and CAF (caffeine, $\delta^{13}C = -38.2‰ \pm 0.10‰$) and the international reference material LVal (L-Valine, USGS73, $\delta^{13}C = -24.03‰ \pm 0.04‰$) (Schimmelmann et al., 2016). These values have been determined using the VPDB-LSVEC two-points scale (Coplen et al., 2006). Even though the material LSVEC itself is no longer recommended as second anchor material, the scale is still transferable using the various international reference materials that originally have been determined using LSVEC as second anchor (Qi et al., 2021). The software of our IRMS evaluates the original $\delta^{45}$ and $\delta^{46}$ measurements using the $^{17}O$ correction according to the method by Craig (1957), but since our reference materials have been determined using the ion correction method by Brand et al. (2010), all our calibrated results agree with this method of ion correction to <0.01‰.

The reference materials were first dissolved in deionized water (3 μg/μL), and then the solutions were loaded on the quartz filter

(Whatman®, GE, pre-cleaned at 650 °C for 2 h), dried at 110 °C and combusted into $CO_2$ for $^{13}C$ analysis. The CAN and CAF were measured at least once per day, and LVal was analyzed at least twice per day. The $\delta^{13}C$ values of the reference materials measured during one week were averaged and used in the linear fit for the calibration valid for the same week. One $\delta^{13}C$ value of LVal was used for calibration, while the other one was used as a quality control (QC) sample for the evaluation of uncertainties and potential drifts occurring over days or long-term periods. The calibrated $\delta^{13}C$ values of these QC LVal from June to August 2019 are shown in Fig. S4. Both the drift and reproducibility (standard deviation of 0.13‰) are fully acceptable.

In this study, $\delta^{13}C$ with a subscript of carbon fractions denotes the $\delta^{13}C$ value of that fraction, e.g. $\delta^{13}C_{EC}$, $\delta^{13}C_{TC}$. Most measurements were repeated more than 3 times, and the standard deviation was used for measurement uncertainty. For the samples measured less than 3 times (e.g. due to limited availability of sample materials), the uncertainties are assumed to be the long-term variability in the measurements of QC LVal standard.

### 2.4. Pyrolysis tests

Some organic materials were selected as test compounds: sucrose, humic acid (HA), humic acid sodium salt (HASS) from Sigma-Aldrich, Suwannee River Fulvic Acid Standard III (SRFA) and Elliott Soil Fulvic Acid Standard V (ESFA) from the International Humic Substances Society. These organic compounds vary in molecular weight and water-solubility, and can represent different organic aerosol components. HA (water-insoluble) and HASS (water-soluble) are used as representative compounds for high molecular weight OC that are known to pyrolyze substantially during thermal desorption. Sucrose (water-soluble) is representative of easily pyrolyzed small molecules. SRFA and ESFA (water-soluble) are easily pyrolyzed with intermediate molecular weight. These water-soluble organic compounds were weighted and dissolved in a known volume of deionized water (Table S5). For each measurement, a certain amount of solution was taken by pipette and then loaded on a quartz filter. The water-insoluble HA was dispersed in 20:80 ethanol/water solution and sonicated in an ultrasonic bath for 5 min, before it was loaded on the quartz filter. More details can be found in Supporting Information Section S4.

The EUSAAR_2 protocol was used for pyrolysis tests. The materials in the pyrolysis tests are all organic (without EC), so TOC is defined as total organic carbon to distinguish from TC. Similarly, pOC in the pyrolysis tests is defined as the fraction collected from the start of the $He/O_2$ phase to the end. Despite not being EC, pOC_split is defined as a part of pOC that evolved after the split time.

### 2.5. EC separation tests

To investigate if the thermal-optical OC/EC split point can be used to isolate EC for $^{13}C$ analysis, EC separation tests were conducted with mixtures of carbon black (Nano-powder, Sigma-Aldrich) and the organic materials above. Carbon black (CB) is used as a surrogate of aerosol EC, because the composition and size of CB particles is similar to aerosol EC, including graphite and a variety of carbon crystals. The CB suspension was prepared using the same method as water-insoluble HA. The organic solutions and CB suspension were then mixed and loaded on the quartz filter. The EUSAAR_2 protocol was used to analyze these filters with mixtures. It is anticipated that if the EC separation is successful, the EC amount should correspond to the CB amount in the solution and $\delta^{13}C_{EC}$ to the delta value of the pure carbon black material ($\delta^{13}C_{CB}$).

The amount of CB deposited on the filter cannot be controlled precisely, because the CB concentration in the suspension is non-uniform and changes with time. However, the CB concentration can be calculated as the difference between the measured TC of the total mixture ($TC_{mixture}$; thermal-optical analyzer) and the known concentration of the water-soluble organic compounds (TOC) in the solution. The EC recovery can be calculated by dividing the separated EC (thermal-optical analyzer) by the CB concentration deposited on the filter:

$$\text{EC recovery} = \frac{\text{EC}}{\text{TC}_{\text{mixture}} - \text{TOC}} \times 100\% \quad (2)$$

### 2.6. $^{13}C$ analysis of biomass-burning source samples and ambient aerosol samples

Biomass-burning source samples and ambient aerosol samples were analyzed for the first application of the new method. Biomass-burning experiments were conducted in the Center for Physical Sciences and Technology (FTMC, Vilnius, Lithuania). For burning experiments, particulate matter with aerodynamic diameter less than 1 μm ($PM_1$) was collected on filters for 15 min each, using a Digitel DH77 aerosol sampler at a flow rate of 500 L/min. Samples from burning of pine and oak wood (both C3 plants) were selected as typical source samples, named PINE and OAK.

Typical European ambient aerosol samples were taken from the Cesar Observatory in the western part of the Netherlands in 2011. The site is between the cities Utrecht and Rotterdam, and not far from the cities The Hague, Leiden and Amsterdam, and therefore represents the regional background of a polluted area in western Europe. $PM_{2.5}$ samples were collected with a high-volume sampler (Digitel DHA-80) at a flow rate of 500 L/min for several days (variable among seasons). Two samples in summer and winter were selected for detailed analysis, named NL-summer and NL-winter, respectively.

Typical Chinese ambient aerosol samples were collected in the urban area of Xi'an City on a building rooftop of the Institute of Earth Environment, Chinese Academy of Sciences. The sampling site is around 15 km south of downtown and surrounded by a residential area with no major industrial activities, and represents a regional background in a typical inland city in central China. $PM_{2.5}$ samples were collected with 24 h duration using a high-volume sampler (TE-6070 MFC, Tisch Inc., Cleveland, OH, USA) at 1.0 $m^3$/min every sixth day from 5 July 2008 to 27 June 2009. Two samples collected in spring and winter were selected as typical samples of polluted seasons, named CN-spring and CN-winter.

The biomass-burning source samples and ambient aerosol samples were collected on precleaned quartz filters, kept in pre-baked aluminium foil and stored at −20 °C before analysis. More sampling information can be found in Tables S6–S8, and air mass trajectories of the aerosol samples can be found in Figs. S5–S6.

These samples were analyzed using the EUSAAR_2 protocol for $\delta^{13}C_{TC}$ and $\delta^{13}C_{EC}$. The $\delta^{13}C_{OC}$ can be measured directly or calculated from $\delta^{13}C_{TC}$ and $\delta^{13}C_{EC}$ based on the isotopic mass balance:

$$\delta^{13}C_{OC} = \left(TC \times \delta^{13}C_{TC} - EC \times \delta^{13}C_{EC}\right)/OC \quad (3)$$

However, the opposite, calculating $\delta^{13}C_{EC}$ from $\delta^{13}C_{TC}$ and $\delta^{13}C_{OC}$ is not feasible, because calculating $\delta^{13}C$ of a small fraction from the difference between two larger quantities will cause large uncertainties, and the detailed explanation can be found in Figs. S9–S10.

To further investigate pOC/EC separation as well as the isotopic composition of pOC and EC, first pOC + EC is collected from the start of the $He/O_2$ phase (where the desorbed OC had been removed in He, but pOC has not yet been oxidized). Subsequently, the carbon fraction that remains at various times after the start of the $He/O_2$ phase in the EUSAAR_2 protocol (referred to as remaining carbon, RC) was collected and measured for $\delta^{13}C$. As pOC is gradually oxidized (potentially along with the least refractory EC) and finally EC is also combusted, RC represents the transition from pOC + EC to EC to more refractory EC.

### 2.7. Dual-isotope source apportionment of aerosol EC

Dual-isotope source apportionment of aerosol EC was conducted based on the following equations.

$$EC = EC_{coal} + EC_{traffic} + EC_{C3} + EC_{C4} \quad (4)$$

$$EC \times F^{14}C_{EC} = (EC_{coal} + EC_{traffic}) \times F^{14}C_{fossil} + (EC_{C3} + EC_{C4}) \times F^{14}C_{non-fossil} \quad (5)$$

$$EC \times \delta^{13}C_{EC} = EC_{coal} \times \delta^{13}C_{coal} + EC_{traffic} \times \delta^{13}C_{traffic} + EC_{C3} \times \delta^{13}C_{C3} + EC_{C4} \times \delta^{13}C_{C4} \quad (6)$$

The $^{14}C$ data (reported as fraction modern, $F^{14}C$) of the aerosol samples were obtained in a previous study (Ni et al., 2018). The *simmr* package (Parnell et al., 2010) in R software was used for the $^{13}C$-$^{14}C$ source apportionment, in which Bayesian Markov chain Monte Carlo (MCMC) was used to propagate uncertainties. The $^{13}C$ source signatures of EC for coal combustion (−23.4‰ ± 1.3‰), traffic emissions (−25.5‰ ± 1.3‰), and C3 plant burning (−26.7‰ ± 1.8‰) come from Andersson et al. (2015) and references therein, and $^{13}C$ source signature of EC for C4 plant burning (−16.4‰ ± 1.4‰) comes from Ni et al. (2018) and references therein. The emissions from fossil sources are $^{14}C$-free, whereas non-fossil emissions contain the contemporary $^{14}C$ content ($F^{14}C_{fossil}$ = 0, $F^{14}C_{non\text{-}fossil}$ = 1.10 ± 0.05; Lewis et al., 2004; Mohn et al., 2008; Palstra and Meijer, 2014; Ni et al., 2019).

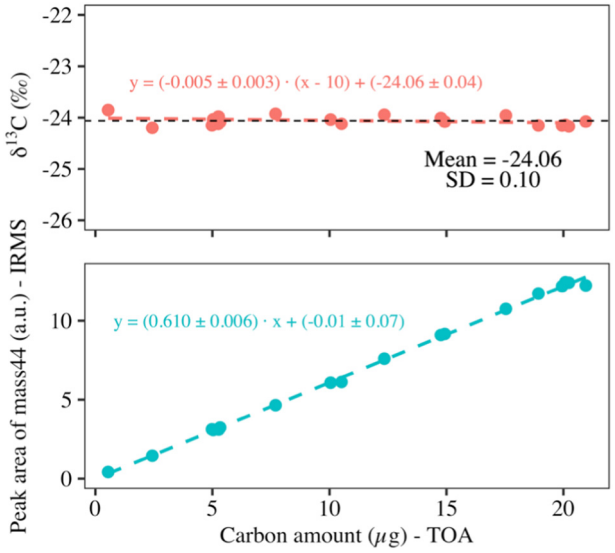


**Fig. 2.** $^{13}C$ mass dependence based on measurements of the standard material LVal (upper panel) and the correlation between carbon amount measured by the TOA and IRMS peak area (lower panel). The red symbols show the $\delta^{13}C$ of LVal with different carbon amounts determined by TOA, and the red dashed line shows a linear regression to the data points. The black dashed line is the average of $\delta^{13}C$ values. Blue symbols show the sample transfer from TOA to IRMS, and the blue dashed line shows the related linear regression.

## 3. Results and discussion

### 3.1. Detection limit, reproducibility, and mass dependence

The limit of detection (LOD) is 0.27 μgC and 0.08 μgC for TOA and IRMS, respectively, and we use 0.30 μgC for the LOD of the whole system (Supporting Information Section S3.3), based on measurements of the LVal standard. In practice, for aerosol filter samples, the measurement range is 1–20 μgC, considering potential filter contamination during sampling and handling. Since the sampling blank usually contains only OC, measurements of EC at sub-μgC level is still possible.

Fig. 2 shows that the $\delta^{13}C$ value is nearly independent of the carbon amount (upper panel), and the carbon mass detected by TOA is linearly related to IRMS peak area with an insignificant intercept (lower panel). $\delta^{13}C$ values of TC analyzed by the TOA-IRMS system are compared with an elemental analyzer (EA) - IRMS in Fig. S3, for 12 different ambient aerosol samples. The averaged difference is −0.08‰ ± 0.06‰ (standard error of the mean), showing that the TOA-IRMS method compares favorably to a standard method for $^{13}C$ analysis of TC.

For $^{13}C$ analysis of TC using EA-IRMS, various measurement ranges are reported, such as 0.5–20 mg (Kawashima and Haneishi, 2012) and 10–40 μgC (Martinsson et al., 2017). Liquid chromatography (LC) - IRMS for water-soluble OC (WSOC) achieves sub-μgC LOD levels, for example, 0.222 μgC with 0.6‰ accuracy (Suto and Kawashima, 2018), 0.114 μgC using online wet oxidation (Morera-Gómez et al., 2021), 0.12 μgC for 0.2‰ precision or 0.012 μgC for 1‰ precision (Sessions et al., 2005). The lowest LOD reported is achieved by the laser ablation (LA) - IRMS, such as 0.024 μgC with 1‰ precision or 0.042 μgC with 0.41‰ precision (van Roij et al., 2017), and 0.0004 μgC with standard deviation of 0.25‰ (Rodionov et al., 2019). However, the EA-IRMS, LC-IRMS, LA-IRMS, or other IRMS systems are not used for $^{13}C$ analysis of EC. The commonly used OC/EC separation methods (Huang et al., 2006; Fisseha et al., 2009; Cao et al., 2011; Chen et al., 2013) are all offline, where glass containers or flame-sealed tubes are needed to store $CO_2$ for independent $^{13}C$ analysis. The sub-μgC LOD of TOA-IRMS is therefore a considerable advance in $^{13}C$ analysis of EC.

With the low detection limit, our method can make use of valuable aerosol filters more efficiently, and allows $^{13}C$ analysis of EC on lightly-loaded filter samples, which originate from very clean areas, e.g., glacier (Li et al., 2016) and polar regions (Winiger et al., 2016). This method is also promising for shorter sampling time or high time resolution, thus making real-time observation possible. The transfer interface can be an option for online $^{13}C$ measurement with an online model TOA. There are currently some meaningful efforts investigating the online $^{13}C$ measurement of ambient aerosol using optical equipment (cavity ring-down spectroscopy, CRDS) (Lin et al., 2020), which also emphasizes the importance and urgency of online $\delta^{13}C$ measurement with reliable OC/EC separation.

### 3.2. Pyrolysis and isotope fractionation in thermal desorption

Isotope fractionation in thermal desorption and pyrolysis may cause a difference in $\delta^{13}C$ of desorbed OC and pOC. To study the extent of pyrolysis and the associated isotope fractionation, we conducted tests, using organic compounds with different molecular weights and water-solubility, including sucrose, humic acid (HA), humic acid sodium salt (HASS), Suwannee River Fulvic Acid Standard III (SRFA), and Elliott Soil Fulvic Acid Standard V (ESFA).

Sucrose was investigated as a surrogate compound (Huang et al., 2006) for non-volatile, small-molecular organic compounds in the atmosphere. In Fig. 3, roughly 80% of the sucrose is desorbed whereas 20% undergoes pyrolysis. pOC is depleted in $^{13}C$ compared to TOC, and the $\delta^{13}C$ difference between pOC and desorbed OC is estimated based on isotopic mass balance to be around 1‰. With all pOC of sucrose combusted before the split time, even though pyrolysis and associated isotope fractionation occurred, any EC collected after the split time would not be affected. Other non-volatile small-molecular organic compounds, such as the lab $^{13}C$ references CAN/CAF/LVal and oxalic acid, do not show pyrolysis in thermal desorption.

The macromolecular organic compounds show a high degree of pyrolysis during thermal desorption in the He phase, with pOC ranging from 50%–60% of TOC for two fulvic acids (ESFA and SRFA) to almost 80% of TOC for humic acids (HASS and HA). Due to such high degree of pyrolysis, only a small fraction of organics was actually desorbed, so the $\delta^{13}C$ of the desorbed part may not be representative for OC any more. Still, for most of macromolecular organic compounds tested, the

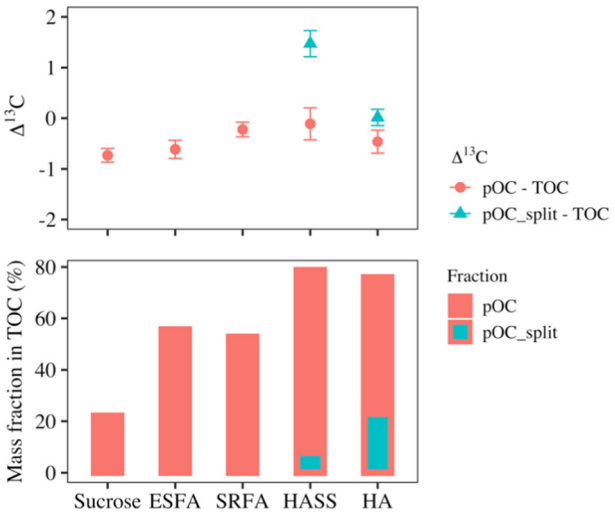


**Fig. 3.** The isotope fractionation during thermal desorption of pure organic materials. The symbols show the $\delta^{13}C$ differences ($\Delta^{13}C$) between pOC and total organic carbon (TOC). pOC refers to pyrolyzed OC collected from the beginning to the end of the EUSAAR_2 $He/O_2$ phase (red), and pOC_split refers to pyrolyzed OC evolved after the split time (green). The bars give the carbon mass fractions as percentage of TOC. The measurements were repeated at least three times, and the error bars represent the standard deviation.

difference of $\delta^{13}C_{pOC}$ and $\delta^{13}C_{TOC}$ is lower than 0.5‰, indicating minor influence of isotope fractionation during thermal desorption with the mild heating steps of EUSAAR_2 protocol. Only the difference between $\delta^{13}C_{pOC}$ and $\delta^{13}C_{TOC}$ of ESFA is larger (0.6‰). All pOC of ESFA and SRFA is combusted before the split time. But this is not the case for HA and HASS, for which approximately 23% and 8% of TOC respectively, evolve after the split time (pOC_split) and may be identified as EC, thus affecting the $\delta^{13}C_{EC}$ determination in aerosol samples. This is due to the fact that HA and HASS is light-absorbing, whereas the concept of the optical split point assumes that organic materials are not light-absorbing. The pOC_split of HA and HASS is enriched in $^{13}C$ compared to pOC, presumably due to isotope fractionation during the continuing oxidation of pOC in $He/O_2$ phase, causing the remaining pOC to be more and more enriched (kinetic fractionation in Fig. S11). The optical correction prevents the majority (up to 100% for ESFA and SRFA, around 90% for HASS and 70% for HA) of the pOC to be counted as EC, but still does not perform optimally for all of these macromolecular organic compounds. However, without this optical correction, EC measured in aerosol samples can contain a considerable amount of pOC of macromolecules, and the $\delta^{13}C_{EC}$ determination will thus be affected.

There is not a consistent trend in the isotope fractionation, with pOC depleted and pOC_split enriched in $^{13}C$ compared to TOC of HA and HASS. The EUSAAR_2 protocol is designed to minimize pyrolysis and uses several gradually rising temperature steps to desorb OC, while some thermal protocols with intense heating may lead to more severe pyrolysis and isotope fractionation. More comparisons between mild or severe heating protocols can be found in Figs. S7–S10, in which the trends of isotope fractionation can be different.

In general, pyrolysis is significant for macromolecules, but less for small molecules. The $\delta^{13}C$ difference between desorbed OC and pOC is usually less than 1‰. Considering that OC in aerosol samples contains only a fraction of macromolecular organic compounds, such as the humic-like compounds (HULIS) (Graber and Rudich, 2006), the influence of pyrolysis is smaller for aerosols than for the pure test compounds. On the other hand, $^{13}C$ analysis of sediments and soils may require more attention due to the considerable amount of HULIS.

### 3.3. EC separation tests

Mixtures of carbon black (CB) powder and organic compounds were analyzed to investigate the OC/EC separation. If the EC separation is successful, the amount of EC isolated according to EUSAAR_2 should correspond to the amount of CB in the mixture and, in addition, the $\delta^{13}C$ value of the isolated EC should correspond to $\delta^{13}C$ of the pure CB material. On the other hand, if the EC isolated after the split time is still mixed with substantial amounts of pOC, one would expect EC to be enriched in $^{13}C$ for HA, HASS, and especially sucrose mixtures, which have less negative $\delta^{13}C$ values than CB. In contrary, EC should be depleted in $^{13}C$ for the SFRA mixture, which has a more negative $\delta^{13}C$ value than CB.

In Fig. 4, EC recoveries being around 100% (±5%) shows that the isolated EC mass corresponds well to the mass of CB in the solution. The isotope values (upper panel) show that the separated EC is always slightly depleted in $^{13}C$ compared to CB, even if the organic compounds in the mixture (blue symbols) are enriched in $^{13}C$. This indicates that pOC does not affect $\delta^{13}C$ of the separated EC after the split time. A part of pOC evolved after the split time in the pyrolysis tests (pOC_split, Fig. 3) with pure HA and HASS. However, in the EC separation tests, no pOC seems to have evolved after the split time, since both mass and $\delta^{13}C$ values of the separated EC closely reflect the original CB. A possible explanation is that compared to the light absorption of CB, the light absorption of HA and HASS is negligible, or that pOC formed in the presence of EC has different thermal properties.

The depletion in $^{13}C$ of the separated EC from the mixtures compared to the original CB is small but statistically significant. However, if $\delta^{13}C_{EC}$ is analyzed from a pure CB suspension, the values agree with $\delta^{13}C$ of CB material within uncertainties. Therefore, the difference observed in the mixtures suggests an unknown isotope fractionation. So far, we cannot explain this deviation and the mechanism needs further investigation. However, the difference in $\delta^{13}C$ between the recovered EC and the original CB is smaller than 0.6‰, which should allow for reasonable source apportionment.

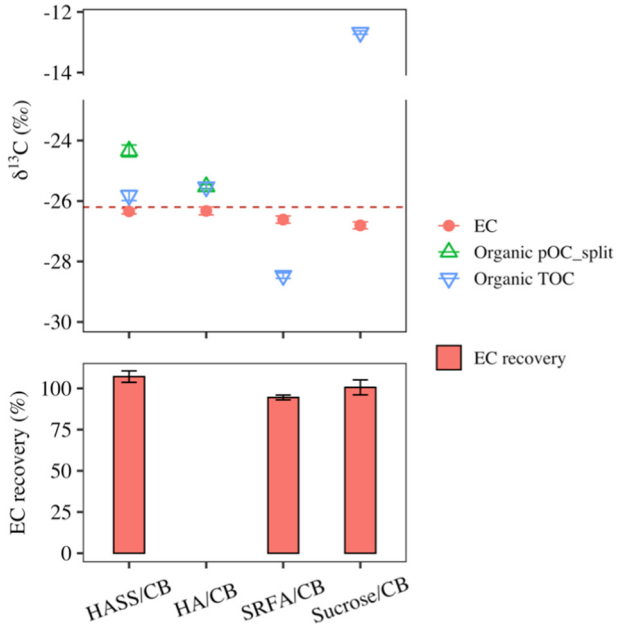


**Fig. 4.** Analysis of $\delta^{13}C_{EC}$ isolated from mixtures of carbon black (CB) with various organic materials with different $\delta^{13}C$ values. The dashed line indicates the nominal $\delta^{13}C$ value of the pure CB material ($\delta^{13}C_{CB} = -26.19‰ \pm 0.13‰$). EC (red symbols) refers to the $\delta^{13}C$ of carbon evolved after the OC/EC split time. Organic pOC_split (green symbols) refers to the $\delta^{13}C$ of pOC evolved after the split time, as measured in Section 3.2. Organic TOC (blue symbols) refers to the $\delta^{13}C$ value of the pure organic compounds, as measured in Section 3.2. EC recovery (red bars) is the mass of isolated EC relative to the mass of CB contained in the mixture (Eq. (2)).

### 3.4. $^{13}C$ analysis of biomass-burning source samples and ambient aerosol samples

After investigating the EC separation on idealized test substances, we apply the method to more realistic aerosol samples, namely biomass-burning source samples and typical ambient filter samples. To investigate the influence of pOC and isotope fractionation on the determination of $^{13}C$ source signature of EC, two biomass-burning (C3 plant) source samples were analyzed for $\delta^{13}C$ values of TC, EC, and pOC + EC, where pOC + EC is collected at the start of the $He/O_2$ phase. In the lower panel of Fig. 5a, pOC accounts for roughly 20% of TC, with concentrations comparable to EC or even higher.

The upper panel of Fig. 5a shows the isotopic composition of TC, EC, and pOC + EC. The latter is representative of a mixture of EC with the pOC that formed during the desorption of OC. For both wood species, $\delta^{13}C_{EC}$ (−27.24‰ ± 0.13‰ for PINE and −28.09‰ ± 0.13‰ for OAK) is lower than $\delta^{13}C_{TC}$ (−26.34‰ ± 0.20‰, −27.62‰ ± 0.23‰). This implies that $\delta^{13}C_{OC}$ (calculated by isotopic mass balance) is higher than $\delta^{13}C_{EC}$, with a difference of around 1‰. $\delta^{13}C_{TC}$ is hence not necessarily representative for $^{13}C$ signatures of EC in wood burning emissions. The difference in $\delta^{13}C$ between OC and EC indicates that different components of the biomass, with different $\delta^{13}C$ values, such as cellulose or fatty acids, may contribute differently to the emitted OC and EC, and/or that isotope fractionation happened during combustion of the biomass. On the other hand, $\delta^{13}C_{pOC+EC}$ is similar to $\delta^{13}C_{EC}$. Previous methods using different OC/EC separation protocols also found $\delta^{13}C_{EC}$ of biomass-burning emissions from C3 plants in a similar range (Kawashima and Haneishi, 2012; Guo et al., 2016).

To investigate the influence of possible different EC isolation methods on $\delta^{13}C_{EC}$, we designed a sensitivity analysis. As each method collects slightly different fractions of EC and potentially pOC, we collected the carbon fraction that remains at various times after the start of the $He/O_2$ phase in the EUSAAR_2 protocol for $^{13}C$ analysis. This fraction is referred to as remaining carbon (RC). RC collected at increasing analysis times represents the transition from pOC + EC, to EC at the split time, to more refractory EC after the split time.

In the lower panel of Fig. 5b, the bars represent how much RC (as percentage of TC) remains on the filter at the respective protocol running time. The $^{13}C$ values in the upper panel represent the isotopic composition of RC at this point in the analysis. The mass fraction of RC decreases with increasing time in the $He/O_2$ phase, as more and more carbon is combusted. At the same time, the corresponding $\delta^{13}C_{RC}$ value changes very little (within 0.5‰). This suggests that pOC and EC from biomass burning emissions have similar $\delta^{13}C$ values, and that gradual oxidation of EC at later stages during the analysis does not have a strong kinetic isotope effect. pOC and EC will never be perfectly separated, since some native EC could evolve before the split time and some pOC after the split time, but this will not strongly impact the $^{13}C$ signature for these source samples. Therefore, we conclude that $\delta^{13}C_{EC}$ of C3 plant burning obtained by other methods should be comparable among each other and to the current method. Also, variations in the split time, which are common among different thermal-optical protocols, will not strongly influence $\delta^{13}C_{EC}$. Similarly, $\delta^{13}C_{OC}$ can also be influenced by the formation of pOC and isotope fractionation, and these impacts are small but not negligible in our cases as shown in Fig. S9.

Compared with source samples, the results are different for ambient aerosol samples, for which the chemical and $^{13}C$ isotopic composition are more complex. Typical aerosol samples from the Netherlands and China were investigated. The lower panel of Fig. 6a shows the mass fractions of EC and pOC in TC. EC accounts for 17%–30% of TC, whereas pOC accounts for roughly 27%–41%, a higher percentage than for biomass burning emissions. Using the same thermal-optical method, pOC is higher in Chinese samples than Dutch samples, indicating that Chinese aerosols are easier to pyrolyze, especially in winter.

The $\delta^{13}C_{EC}$ value of NL-winter (−26.68‰) is higher than $\delta^{13}C_{TC}$. The $\delta^{13}C_{EC}$ values for NL-summer (−27.42‰), CN-spring (−26.53‰), and CN-winter (−25.74‰) are all lower than the corresponding $\delta^{13}C_{TC}$. The differences between $\delta^{13}C_{TC}$ and $\delta^{13}C_{EC}$ are not negligible (−0.57‰ to 1.43‰). More importantly, the difference between $\delta^{13}C_{EC}$ and $\delta^{13}C_{pOC+EC}$ is 0.16‰ for NL-summer, 0.60‰ for NL-winter, −0.49‰ for CN-spring, and −1.52‰ for CN-winter. This suggests that pOC and EC can differ in $^{13}C$ isotopic composition for ambient samples. Therefore, $\delta^{13}C_{EC}$ can be influenced significantly, if EC is mixed with a considerable fraction of pOC, so the optical pOC compensation is important for ambient aerosol samples.

The low LOD of TOA-IRMS allows dozens of measurement repetitions for one single filter, so the pOC/EC sensitivity analysis can be also conducted in ambient aerosol samples, as shown in Fig. 6b. After the start of the $He/O_2$ phase, the RC remaining on the filter decreases with increasing protocol running time at similar rate of the biomass-burning samples. Different from the biomass-burning samples, the

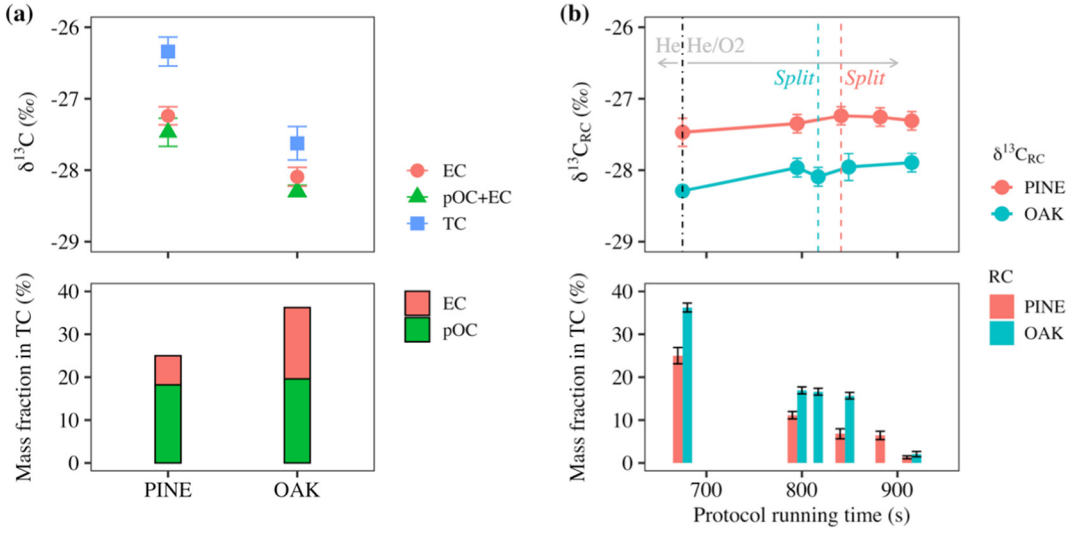


**Fig. 5.** The $^{13}C$ analysis of biomass-burning (C3 plant) source samples based on the EUSAAR_2 protocol. (a) The symbols show the $\delta^{13}C$ of various carbon fractions, including EC (red), pOC + EC (green) and TC (blue). The bars refer to the mass fractions of EC and pOC in TC. (b) The $\delta^{13}C$ values (symbols) and mass fractions of remaining carbon (RC, bars) captured at various times from the start of the $He/O_2$ phase to the end. The carrier gas changing from He to $He/O_2$ is marked by the black dash-dot line. The OC/EC split time of each sample is marked by respective colored dashed lines.

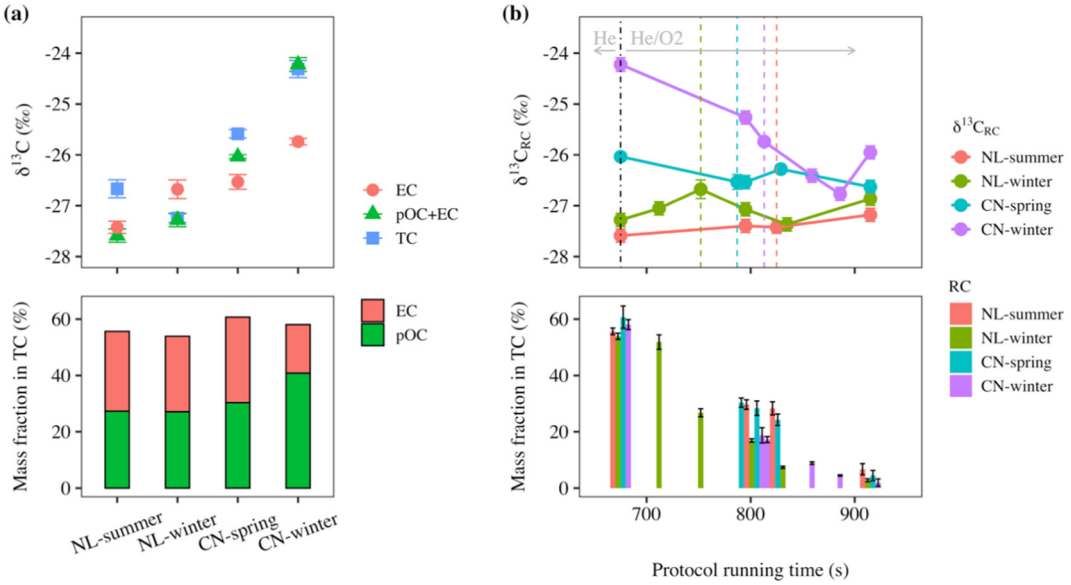


**Fig. 6.** The $^{13}C$ analysis of ambient aerosol samples based on the EUSAAR_2 protocol. (a) The symbols show the $\delta^{13}C$ of various carbon fractions, including EC (red), pOC + EC (green) and TC (blue). The bars refer to the mass fractions of EC and pOC in TC. (b) The $\delta^{13}C$ values (symbols) and mass fractions of remaining carbon (RC, bars) captured at various times from the start of the He/$O_2$ phase to the end. The carrier gas change from He into He/$O_2$ is marked by the black dash-dot line. The OC/EC split time of each sample is marked by respective colored dashed lines.

$\delta^{13}C_{RC}$ of the ambient aerosol samples varies more strongly with increasing analysis time. The $\delta^{13}C_{RC}$ of the NL-summer and CN-spring samples change insignificantly with increasing time in the He/$O_2$ phase, but the $\delta^{13}C_{RC}$ of CN-winter decreases continuously. The $\delta^{13}C_{RC}$ of NL-winter increases before the split time and decreases thereafter.

Between the start of the He/$O_2$ phase (dot-dashed line) and the respective split point, the major fraction of the pOC should be combusted and the trend in $\delta^{13}C_{RC}$ up to the split time is consistent with this: for Chinese samples, OC is enriched in $^{13}C$ compared to EC (Fig. 6a, isotopic mass balance), and therefore pOC is likely enriched as well. As a consequence, RC should become depleted in $\delta^{13}C$ as more of the pOC is removed. This is consistent with the decreasing trend of $\delta^{13}C_{RC}$ from the start of the He/$O_2$ phase to the split time. On the contrary, for NL-winter, OC is depleted with respect to TC and $\delta^{13}C_{RC}$ gradually increases towards the split time, as pOC with a low $\delta^{13}C$ value getting removed.

Changes in $\delta^{13}C_{RC}$ are 0.26‰, 0.50‰, and 0.87‰ for NL-summer, NL-winter, and CN-spring, respectively, whereas $\delta^{13}C_{RC}$ of CN-winter changes by 2.5‰. Based on the $\delta^{13}C$ trend of CN-winter after the split time, it is not likely that the change in $\delta^{13}C$ is due to kinetic fractionation during oxidation of the EC, as in this case we would expect the remaining EC to be gradually enriched in $^{13}C$. A more likely explanation is that EC from different sources has both different thermal stability and $\delta^{13}C$ values. For example, EC from coal combustion, which is enriched in $^{13}C$, might be removed from the filter earlier in the analysis than traffic EC. Then a larger fraction of traffic EC remains on the filter with increasing analysis time, which would explain the trend towards more depleted values of RC. This means that the timing of the OC/EC split can then have significant impact on $\delta^{13}C_{EC}$ and in such cases should be carefully checked.

### 3.5. Source apportionment of aerosols samples

To demonstrate how including pOC into EC can affect source apportionment, we conduct a sensitivity study for the Chinese samples. We do not consider the Dutch samples, since the $^{13}C$ source signatures of EC in the Netherlands are not well known. In Fig. 7a, the $\delta^{13}C_{EC}$ and $\delta^{13}C_{pOC+EC}$ of the Chinese aerosol samples are compared with typical $^{13}C$ source signatures of EC from literature (Andersson et al., 2015; Ni

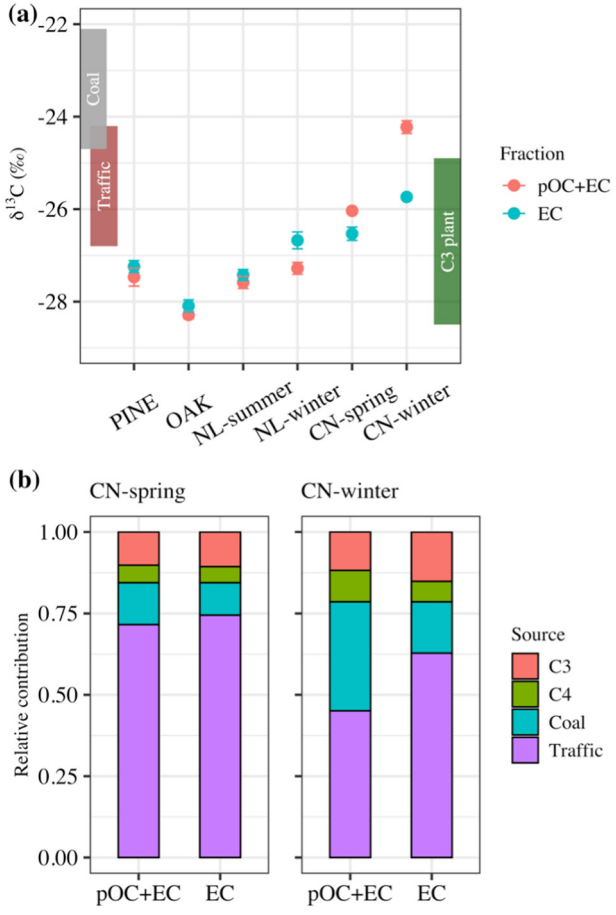


**Fig. 7.** (a) $\delta^{13}C_{EC}$ and $\delta^{13}C_{pOC+EC}$ values of biomass-burning samples and ambient aerosol samples. The colored vertical boxes indicate $^{13}C$ source signatures from literature (C4 plant is out of the y scale, −16.4‰ ± 1.4‰). (b) $^{13}C$-$^{14}C$ source apportionment of EC in sample CN-spring and CN-winter, which was collected in Xi'an, China.

et al., 2018). The $\delta^{13}C_{EC}$ values of CN-spring and CN-winter are located between $\delta^{13}C_{EC}$ ranges of traffic and C3 plant burning emissions, but $\delta^{13}C_{pOC+EC}$ value of CN-winter is closer to the $\delta^{13}C_{EC}$ range of coal combustion, indicating that pOC of CN-winter may be related to coal combustion. A previous study suggests that coal combustion is the main source of OC in winter in Xi'an, China (Ni et al., 2018). However, the $^{13}C$-enriched pOC does not necessarily come from the pyrolysis of $^{13}C$-enriched coal OC, and it can also come from the $^{13}C$ enrichment of aerosol aging (Pavuluri and Kawamura, 2012) or other atmospheric processes (Kirillova et al., 2013).

To further investigate the influence of different separation methods and thus $\delta^{13}C_{EC}$ determination on source apportionment, a Baysian MCMC source apportionment was done for CN-spring and CN-winter using first $\delta^{13}C_{pOC+EC}$ and then $\delta^{13}C_{EC}$. In this case, $\delta^{13}C_{EC}$ is representative of thermal-optical methods and $\delta^{13}C_{pOC+EC}$ is represents an extreme case of methods that do not separate pOC from EC. Fig. 7b compares the relative contribution of 4 sources to pOC + EC and EC (the best estimate; the full probability distributions in Fig. S12). For CN-spring, the coal and traffic contributions would be over- and underestimated by around 4% (coal from 10.3% to 13.7%; traffic from 74.1% to 70.7%), if pOC and EC would not be separated but all assumed to be EC. However, the over- and underestimation could reach 20% for CN-winter (coal from 14.9% to 34.7%; traffic from 63.6% to 43.6%) if all pOC would be allocated to EC. The contribution of biomass burning is less influenced (16% in both cases of CN-spring; 21% in both cases of CN-winter), since it is well-constrained by $^{14}C$. The larger over- and underestimation of coal and traffic contributions of sample CN-winter come from the larger share of pOC with larger $\delta^{13}C$ difference between pOC and EC. On the other hand, if the OC lacks the pOC part, the $\delta^{13}C_{OC}$ determination can also be influenced (Fig. S9). In summary, the optical pOC compensation is necessary for aerosol $^{13}C$ analysis.

## 4. Conclusions

The Sunset thermal-optical analyzer and IRMS are coupled and modified to enable the thermal-optical OC/EC separation for $^{13}C$ analysis at the sub-μgC level. With online separation, combustion, and purification, the transfer interface is applicable for online measurement, possibly even in the field. The influence of pyrolysis and isotope fractionation on $\delta^{13}C_{EC}$ was investigated using various organic compounds and their mixtures with carbon black (a surrogate of EC). The EC separated by the thermal-optical method was comparable to CB in the mixture, both in amount as well as in $^{13}C$ isotopic composition.

A first application to C3 biomass-burning samples indicates that $\delta^{13}C_{TC}$ can be different from $\delta^{13}C_{EC}$, so it cannot be safely used as a substitute for $\delta^{13}C_{EC}$. On the other hand, the influence of pOC on $\delta^{13}C_{EC}$ is negligible (within 0.5‰), which means $\delta^{13}C_{EC}$ signatures of C3 plants obtained by various OC/EC separation methods should be comparable. Contrary to the source samples, for ambient aerosol samples, $\delta^{13}C_{EC}$ can be significantly altered if pOC is mixed with EC. An incomplete separation of pOC from EC can lead to over- or underestimation of the various sources in a source apportionment calculation.

## CRediT authorship contribution statement

**Peng Yao:** Methodology, Validation, Formal analysis, Investigation, Visualization, Data curation, Writing – original draft, Writing – review & editing. **Haiyan Ni:** Validation, Investigation, Resources, Writing – review & editing. **Dipayan Paul:** Methodology, Validation, Investigation, Writing – review & editing. **Agne Masalaite:** Investigation, Resources, Writing – review & editing. **Ru-Jin Huang:** Conceptualization, Validation, Investigation, Resources, Writing – review & editing, Supervision, Funding acquisition. **Harro A.J. Meijer:** Validation, Investigation, Writing – review & editing. **Ulrike Dusek:** Conceptualization, Methodology, Validation, Investigation, Resources, Writing – review & editing, Supervision, Project administration, Funding acquisition.

## Declaration of competing interest

The authors declare that they have no known competing financial interests or personal relationships that could have appeared to influence the work reported in this paper.

## Acknowledgment

This work was supported by National Key Research and Development Program of China (grant no. 2017YFC0212701) and the program of China Scholarships Council No. 201806320346. Special thanks are given to Henk Jansen and Marc Bleeker for their help with the system modification and tests at CIO, and to Romke Tjoelker and Katrin Zenker for developing the connection interface at CIO.

## Appendix A. Supplementary data

Supporting Information to this article can be found online at https://doi.org/10.1016/j.scitotenv.2021.150031.

## References

Andersson, A., Deng, J., Du, K., Zheng, M., Yan, C., Sköld, M., Gustafsson, Ö., 2015. Regionally-varying combustion sources of the January 2013 severe haze events over eastern China. Environ. Sci. Technol. 49, 2038–2043. https://doi.org/10.1021/es503855e.

Andreae, M.O., Gelencsér, A., 2006. Black carbon or brown carbon? The nature of light-absorbing carbonaceous aerosols. Atmos. Chem. Phys. 6, 3131–3148. https://doi.org/10.5194/acp-6-3131-2006.

Birch, M.E., Cary, R.A., 1996. Elemental carbon-based method for monitoring occupational exposures to particulate diesel exhaust. Aerosol Sci. Technol. 25, 221–241. https://doi.org/10.1080/02786829608965393.

Brand, W.A., Assonov, S.S., Coplen, T.B., 2010. Correction for the 17O interference in d (13C) measurements when analyzing CO2 with stable isotope mass spectrometry (IUPAC technical Report). Pure Appl. Chem. 82, 1719–1733. https://doi.org/10.1351/PAC-REP-09-01-05.

Cachier, H., Buat-Menard, P., Fontugne, M., Rancher, J., 1985. Source terms and source strengths of the carbonaceous aerosol in the tropics. J. Atmos. Chem. 3, 469–489. https://doi.org/10.1007/BF00053872.

Cao, J., Chow, J.C., Tao, J., Lee, S., Watson, J.G., Ho, K., Wang, G., Zhu, C., Han, Y., 2011. Stable carbon isotopes in aerosols from Chinese cities: influence of fossil fuels. Atmos. Environ. 45, 1359–1363. https://doi.org/10.1016/j.atmosenv.2010.10.056.

Cavalli, F., Viana, M., Yttri, K.E., Genberg, J., Putaud, J.-P., 2010. Toward a standardised thermal-optical protocol for measuring atmospheric organic and elemental carbon: the EUSAAR protocol. Atmos. Meas. Tech. 3, 79–89. https://doi.org/10.5194/amt-3-79-2010.

Chen, Y., Sheng, G., Bi, X., Feng, Y., Mai, B., Fu, J., 2005. Emission factors for carbonaceous particles and polycyclic aromatic hydrocarbons from residential coal combustion in China. Environ. Sci. Technol. 39, 1861–1867. https://doi.org/10.1021/es0493650.

Chen, B., Andersson, A., Lee, M., Kirillova, E.N., Xiao, Q., Kruså, M., Shi, M., Hu, K., Lu, Z., Streets, D.G., Du, K., Gustafsson, Ö., 2013. Source forensics of black carbon aerosols from China. Environ. Sci. Technol. 47, 9102–9108. https://doi.org/10.1021/es401599r.

Chow, J.C., Watson, J.G., Crow, D., Lowenthal, D.H., Merrifield, T., 2001. Comparison of IMPROVE and NIOSH carbon measurements. Aerosol Sci. Technol. 34, 23–34. https://doi.org/10.1080/02786820119073.

Coplen, T.B., Brand, W.A., Gehre, M., Gröning, M., Meijer, H.A.J., Toman, B., Verkouteren, R.M., 2006. New guidelines for d13C measurements. Anal. Chem. 78, 2439–2441. https://doi.org/10.1021/ac052027c.

Craig, H., 1957. Isotopic standards for carbon and oxygen and correction factors for mass-spectrometric analysis of carbon dioxide. Geochim. Cosmochim. Acta 12, 133–149. https://doi.org/10.1016/0016-7037(57)90024-8.

Dusek, U., Meusinger, C., Oyama, B., Ramon, W., de Wilde, P.A., Holzinger, R., Röckmann, T., 2013. A thermal desorption system for measuring d13C ratios on organic aerosol. J. Aerosol Sci. 66, 72–82. https://doi.org/10.1016/j.jaerosci.2013.08.005.

Dusek, U., Monaco, M., Prokopiou, M., Gongriep, F., Hitzenberger, R., Meijer, H.A.J., Röckmann, T., 2014. Evaluation of a two-step thermal method for separating organic and elemental carbon for radiocarbon analysis. Atmos. Meas. Tech. 7, 1943–1955. https://doi.org/10.5194/amt-7-1943-2014.

Fisseha, R., Saurer, M., Jäggi, M., Siegwolf, R.T.W., Dommen, J., Szidat, S., Samburova, V., Baltensperger, U., 2009. Determination of primary and secondary sources of organic acids and carbonaceous aerosols using stable carbon isotopes. Atmos. Environ. 43, 431–437. https://doi.org/10.1016/j.atmosenv.2008.08.041.

Fu, P.Q., Kawamura, K., Chen, J., Li, J., Sun, Y.L., Liu, Y., Tachibana, E., Aggarwal, S.G., Okuzawa, K., Tanimoto, H., Kanaya, Y., Wang, Z.F., 2012. Diurnal variations of organic molecular tracers and stable carbon isotopic composition in atmospheric aerosols

over Mt. Tai in the North China Plain: an influence of biomass burning. Atmos. Chem. Phys. 12, 8359–8375. https://doi.org/10.5194/acp-12-8359-2012.

Fuzzi, S., Baltensperger, U., Carslaw, K., Decesari, S., Denier Van Der Gon, H., Facchini, M.C., Fowler, D., Koren, I., Langford, B., Lohmann, U., Nemitz, E., Pandis, S., Riipinen, I., Rudich, Y., Schaap, M., Slowik, J.G., Spracklen, D.V., Vignati, E., Wild, M., Williams, M., Gilardoni, S., 2015. Particulate matter, air quality and climate: lessons learned and future needs. Atmos. Chem. Phys. 15, 8217–8299. https://doi.org/10.5194/acp-15-8217-2015.

Graber, E.R., Rudich, Y., 2006. Atmospheric HULIS: how humic-like are they? A comprehensive and critical review. Atmos. Chem. Phys. 6, 729–753. https://doi.org/10.5194/acp-6-729-2006.

Guo, Z., Jiang, W., Chen, S., Sun, D., Shi, L., Zeng, G., Rui, M., 2016. Stable isotopic compositions of elemental carbon in PM1.1 in north suburb of Nanjing region. China. Atmos. Res. 168, 105–111. https://doi.org/10.1016/j.atmosres.2015.09.006.

Gustafsson, Ö., Kruså, M., Zencak, Z., Sheesley, R.J., Granat, L., Engström, E., Praveen, P.S., Rao, P.S.P.P., Leck, C., Rodhe, H., 2009. Brown clouds over South Asia: biomass or fossil fuel combustion? Science 323, 495–498. https://doi.org/10.1126/science.1164857.

Habib, G., Venkataraman, C., Bond, T.C., Schauer, J.J., 2008. Chemical, microphysical and optical properties of primary particles from the combustion of biomass fuels. Environ. Sci. Technol. 42, 8829–8834. https://doi.org/10.1021/es800943f.

Hallquist, M., Wenger, J.C., Baltensperger, U., Rudich, Y., Simpson, D., Claeys, M., Dommen, J., Donahue, N.M., George, C., Goldstein, A.H., Hamilton, J.F., Herrmann, H., Hoffmann, T., Iinuma, Y., Jang, M., Jenkin, M.E., Jimenez, J.L., Kiendler-Scharr, A., Maenhaut, W., McFiggans, G., Mentel, T.F., Monod, A., Prévôt, A.S.H.H., Seinfeld, J.H., Surratt, J.D., Szmigielski, R., Wildt, J., 2009. The formation, properties and impact of secondary organic aerosol: current and emerging issues. Atmos. Chem. Phys. 9, 5155–5236. https://doi.org/10.5194/acp-9-5155-2009.

Han, H., Kim, G., Seo, H., Shin, K.-H., Lee, D.-H., 2020. Significant seasonal changes in optical properties of brown carbon in the midlatitude atmosphere. Atmos. Chem. Phys. 20, 2709–2718. https://doi.org/10.5194/acp-20-2709-2020.

Huang, L., Brook, J.R., Zhang, W., Li, S.M., Graham, L., Ernst, D., Chivulescu, A., Lu, G., 2006. Stable isotope measurements of carbon fractions (OC/EC) in airborne particulate: a new dimension for source characterization and apportionment. Atmos. Environ. 40, 2690–2705. https://doi.org/10.1016/j.atmosenv.2005.11.062.

Huang, R., Zhang, Y., Bozzetti, C., Ho, K., Cao, J., Han, Y., Daellenbach, K.R., Slowik, J.G., Platt, S.M., Canonaco, F., Zotter, P., Wolf, R., Pieber, S.M., Bruns, E.A., Crippa, M., Ciarelli, G., Piazzalunga, A., Schwikowski, M., Abbaszade, G., Schnelle-Kreis, J., Zimmermann, R., An, Z., Szidat, S., Baltensperger, U., Haddad, I.El, Prévôt, A.S.H., 2014. High secondary aerosol contribution to particulate pollution during haze events in China. Nature 514, 218–222. https://doi.org/10.1038/nature13774.

Kawashima, H., Haneishi, Y., 2012. Effects of combustion emissions from the Eurasian continent in winter on seasonal d13C of elemental carbon in aerosols in Japan. Atmos. Environ. 46, 568–579. https://doi.org/10.1016/j.atmosenv.2011.05.015.

Kirillova, E.N., Andersson, A., Sheesley, R.J., Kruså, M., Praveen, P.S., Budhavant, K., Safai, P.D., Rao, P.S.P., Gustafsson, Ö., 2013. 13C- and 14C-based study of sources and atmospheric processing of water-soluble organic carbon (WSOC) in South Asian aerosols. J. Geophys. Res. Atmos. 118, 614–626. https://doi.org/10.1002/jgrd.50130.

Kroll, J.H., Seinfeld, J.H., 2008. Chemistry of secondary organic aerosol: formation and evolution of low-volatility organics in the atmosphere. Atmos. Environ. 42, 3593–3624. https://doi.org/10.1016/j.atmosenv.2008.01.003.

Lewis, C.W., Klouda, G.A., Ellenson, W.D., 2004. Radiocarbon measurement of the biogenic contribution to summertime PM-2.5 ambient aerosol in Nashville, TN. Atmos. Environ. 38, 6053–6061. https://doi.org/10.1016/j.atmosenv.2004.06.011.

Li, C., Bosch, C., Kang, S., Andersson, A., Chen, P., Zhang, Q., Cong, Z., Chen, B., Qin, D., Gustafsson, Ö., 2016. Sources of black carbon to the Himalayan-Tibetan Plateau glaciers. Nat. Commun. 7, 12574. https://doi.org/10.1038/ncomms12574.

Lin, Y.C., Zhang, Y.L., Xie, F., Zhang, W.Q., Fan, M.Y., Lin, Z., Rella, C.W., Hoffnagle, J.A., 2020. Development of a monitoring system for semicontinuous measurements of stable carbon isotope ratios in atmospheric carbonaceous aerosols: optimized methods and application to field measurements. Anal. Chem. 92, 14373–14382. https://doi.org/10.1021/acs.analchem.0c02063.

Martinsson, J., Andersson, A., Sporre, M.K., Friberg, J., Kristensson, A., Swietlicki, E., Olsson, P.-A.A., Stenström, K.E., 2017. Evaluation of d13C in carbonaceous aerosol source apportionment at a rural measurement site. Aerosol Air Qual. Res. 17, 2081–2094. https://doi.org/10.4209/aaqr.2016.09.0392.

Masalaite, A., Holzinger, R., Ceburnis, D., Remeikis, V., Ulevicius, V., Röckmann, T., Dusek, U., 2018. Sources and atmospheric processing of size segregated aerosol particles revealed by stable carbon isotope ratios and chemical speciation. Environ. Pollut. 240, 286–296. https://doi.org/10.1016/j.envpol.2018.04.073.

Mohn, J., Szidat, S., Fellner, J., Rechberger, H., Quartier, R., Buchmann, B., Emmenegger, L., 2008. Determination of biogenic and fossil CO2 emitted by waste incineration based on 14CO2 and mass balances. Bioresour. Technol. 99, 6471–6479. https://doi.org/10.1016/j.biortech.2007.11.042.

Morera-Gómez, Y., Cong, Z., Widory, D., 2021. Carbonaceous fractions contents and carbon stable isotope compositions of aerosols collected in the atmosphere of Montreal (Canada): seasonality, sources, and implications. Front. Environ. Sci. 9. https://doi.org/10.3389/fenvs.2021.622521.

Ni, H., Huang, R.-J., Cao, J., Zhang, T., Wang, M., Meijer, H.A.J., Dusek, U., Liu, W., Zhang, T., Wang, M., Meijer, H.A.J., Dusek, U., 2018. Source apportionment of carbonaceous aerosols in Xi'an, China: insights from a full year of measurements of radiocarbon and the stable isotope 13C. Atmos. Chem. Phys. 18, 16363–16383. https://doi.org/10.5194/acp-18-16363-2018.

Ni, H., Huang, R.J., Cao, J., Guo, J., Deng, H., Dusek, U., 2019. Sources and formation of carbonaceous aerosols in Xi'an, China: primary emissions and secondary formation constrained by radiocarbon. Atmos. Chem. Phys. 19, 15609–15628. https://doi.org/10.5194/acp-19-15609-2019.

Norman, A.L., Hopper, J.F., Blanchard, P., Ernst, D., Brice, K., Alexandrou, N., Klouda, G., 1999. The stable carbon isotope composition of atmospheric PAHs. Atmos. Environ. 33, 2807–2814. https://doi.org/10.1016/S1352-2310(98)00358-6.

Palstra, S.W.L., Meijer, H.A.J., 2014. Biogenic carbon fraction of biogas and natural gas fuel mixtures determined with 14C. Radiocarbon 56, 7–28. https://doi.org/10.2458/56.16514.

Parnell, A.C., Inger, R., Bearhop, S., Jackson, A.L., 2010. Source partitioning using stable isotopes: coping with too much variation. PLoS One 5, 1–5. https://doi.org/10.1371/journal.pone.0009672.

Pavuluri, C.M., Kawamura, K., 2012. Evidence for 13-carbon enrichment in oxalic acid via iron catalyzed photolysis in aqueous phase. Geophys. Res. Lett. 39, 1–6. https://doi.org/10.1029/2011GL050398.

Petzold, A., Ogren, J.A., Fiebig, M., Laj, P., Li, S.-M., Baltensperger, U., Holzer-Popp, T., Kinne, S., Pappalardo, G., Sugimoto, N., Wehrli, C., Wiedensohler, A., Zhang, X.-Y., 2013. Recommendations for reporting "black carbon" measurements. Atmos. Chem. Phys. 13, 8365–8379. https://doi.org/10.5194/acp-13-8365-2013.

Qi, H., Moossen, H., Meijer, H.A.J., Coplen, T.B., Aerts-Bijma, A.T., Reid, L., Geilmann, H., Richter, J., Rothe, M., Brand, W.A., Toman, B., Benefield, J., Hélie, J.F., 2021. USGS44, a new high-purity calcium carbonate reference material for d13C measurements. Rapid Commun. Mass Spectrom. 35. https://doi.org/10.1002/rcm.9006.

Rodionov, A., Lehndorff, E., Stremtan, C.C., Brand, W.A., Königshoven, H.-P., Amelung, W., 2019. Spatial microanalysis of natural 13C/12C abundance in environmental samples using laser ablation-isotope ratio mass spectrometry. Anal. Chem. 91, 6225–6232. https://doi.org/10.1021/acs.analchem.9b00892.

Schauer, J.J., Mader, B.T., DeMinter, J.T., Heidemann, G., Bae, M.S., Seinfeld, J.H., Flagan, R.C., Cary, R.A., Smith, D., Huebert, B.J., Bertram, T., Howell, S., Kline, J.T., Quinn, P., Bates, T., Turpin, B., Lim, H.J., Yu, J.Z., Yang, H., Keywood, M.D., 2003. ACE-Asia intercomparison of a thermal-optical method for the determination of particle-phase organic and elemental carbon. Environ. Sci. Technol. 37, 993–1001. https://doi.org/10.1021/es020622f.

Schimmelmann, A., Qi, H., Coplen, T.B., Brand, W.A., Fong, J., Meier-Augenstein, W., Kemp, H.F., Toman, B., Ackermann, A., Assonov, S., Aerts-Bijma, A.T., Brejcha, R., Chikaraishi, Y., Darwish, T., Elsner, M., Gehre, M., Geilmann, H., Gröning, M., Hélie, J.-F.F., Herrero-Martín, S., Meijer, H.A.J.J., Sauer, P.E., Sessions, A.L., Werner, R.A., 2016. Organic reference materials for hydrogen, carbon, and nitrogen stable isotope-ratio measurements: caffeines, n -alkanes, fatty acid methyl esters, glycines, l -valines, polyethylenes, and oils. Anal. Chem. 88, 4294–4302. https://doi.org/10.1021/acs.analchem.5b04392.

Sessions, A.L., Sylva, S.P., Hayes, J.M., 2005. Moving-wire device for carbon isotopic analyses of nanogram quantities of nonvolatile organic carbon. Anal. Chem. 77, 6519–6527. https://doi.org/10.1021/ac051251z.

Smith, B.N., Epstein, S., 1971. Two categories of 13C/12C ratios for higher plants. Plant Physiol. 47, 380–384. https://doi.org/10.1104/pp.47.3.380.

Suto, N., Kawashima, H., 2018. Online wet oxidation/isotope ratio mass spectrometry method for determination of stable carbon isotope ratios of water-soluble organic carbon in particulate matter. Rapid Commun. Mass Spectrom. 32, 1668–1674. https://doi.org/10.1002/rcm.8240.

Szidat, S., Jenk, T.M., Gäggeler, H.W., Synal, H.A., Fisseha, R., Baltensperger, U., Kalberer, M., Samburova, V., Reimann, S., Kasper-Giebl, A., Hajdas, I., 2004. Radiocarbon (14C)-deduced biogenic and anthropogenic contributions to organic carbon (OC) of urban aerosols from Zürich, Switzerland. Atmos. Environ. 38, 4035–4044. https://doi.org/10.1016/j.atmosenv.2004.03.066.

Tao, J., Zhang, L., Cao, J., Zhang, R., 2017. A review of current knowledge concerning PM2.5 chemical composition, aerosol optical properties and their relationships across China. Atmos. Chem. Phys. 17, 9485–9518. https://doi.org/10.5194/acp-17-9485-2017.

van Roij, L., Sluijs, A., Laks, J.J., Reichart, G.J., 2017. Stable carbon isotope analyses of nanogram quantities of particulate organic carbon (pollen) with laser ablation nano combustion gas chromatography/isotope ratio mass spectrometry. Rapid Commun. Mass Spectrom. 31, 47–58. https://doi.org/10.1002/rcm.7769.

Widory, D., 2006. Combustibles, fuels and their combustion products: a view through carbon isotopes. Combust. Theory Model. 10, 831–841. https://doi.org/10.1080/13647830600720264.

Winiger, P., Andersson, A., Eckhardt, S., Stohl, A., Gustafsson, Ö., 2016. The sources of atmospheric black carbon at a European gateway to the Arctic. Nat. Commun. 7, 12776. https://doi.org/10.1038/ncomms12776.

Zencak, Z., Elmquist, M., Gustafsson, Ö., 2007. Quantification and radiocarbon source apportionment of black carbon in atmospheric aerosols using the CTO-375 method. Atmos. Environ. 41, 7895–7906. https://doi.org/10.1016/j.atmosenv.2007.06.006.

Zenker, K., Sirignano, C., Riccio, A., Chianese, E., Calfapietra, C., Prati, M.V., Masalaite, A., Remeikis, V., Mook, E., Meijer, H.A.J., Dusek, U., 2020. d13C signatures of organic aerosols: measurement method evaluation and application in a source study. J. Aerosol Sci. 145, 105534. https://doi.org/10.1016/j.jaerosci.2020.105534.

Zhang, Y.L., Perron, N., Ciobanu, V.G., Zotter, P., Minguillón, M.C., Wacker, L., Prévt, A.S.H., Baltensperger, U., Szidat, S., 2012. On the isolation of OC and EC and the optimal strategy of radiocarbon-based source apportionment of carbonaceous aerosols. Atmos. Chem. Phys. 12, 10841–10856. https://doi.org/10.5194/acp-12-10841-2012.

Zhang, Y., Cai, J., Wang, S., He, K., Zheng, M., 2017. Review of receptor-based source apportionment research of fine particulate matter and its challenges in China. Sci. Total Environ. 586, 917–929. https://doi.org/10.1016/j.scitotenv.2017.02.071.